Mesoporous ZnS–NiS Nanocomposites for Nonenzymatic Electrochemical Glucose Sensors

Chengzhen Wei,[a] Cheng Cheng,[a] Junhong Zhao,[a] Zhangtao Wang,[a] Haipeng Wu,[a] Kaiyue Gu,[a] Weimin Du,[a] and Huan Pang*[a, b]

Mesoporous ZnS–NiS composites are prepared via ion-exchange reactions using ZnS as the precursor. The prepared mesoporous ZnS–NiS composite materials have large surface areas (137.9 m^{2}g^{-1}) compared with the ZnS precursor. More importantly, the application of these mesoporous ZnS–NiS composites as nonenzymatic glucose sensors was successfully explored. Electrochemical sensors based on mesoporous ZnS–NiS composites exhibit a high selectivity and a low detection limit (0.125 μM) toward the oxidation of glucose, which can

mainly be attributed to the morphological characteristics of the mesoporous structure with high specific surface area and a rational composition of the two constituents. In addition, the mesoporous ZnS–NiS composites coated on the surface of electrodes can be used to modify the mass transport regime, and this alteration can, in favorable circumstances, facilitate the amperometric discrimination between species. These results suggest that such mesoporous ZnS–NiS composites are promising materials for nonenzymatic glucose sensors.

Introduction

Over the past years, the design and synthesis of nanostructured materials with desired size, shape, and morphology have attracted considerable attention for achieving novel morphology-dependent chemical–physical properties.[1–8] Particularly, porous nanostructure materials have received significant interest owing to the pore structure features and the large specific surface area, which make them suitable for applications in catalysis, sensing, energy storage, etc.[9–16]

Glucose monitoring is vital in clinical diagnostics, biotechnology, and the food industry. Specifically, there has been great interest in the development of electrochemical glucose sensors.[17] Compared with other detection approaches, the use of an electrochemical technique is one of the most promising in the construction of simple and low-cost glucose sensors because of its high sensitivity, good selectivity, and ease of operation. The conventional glucose biosensors based on glucose oxidase (GOD) exhibit high sensitivity and selectivity. However,

due to the intrinsic features of enzymes, these GOD-based biosensor approaches suffer greatly from the influences of various environmental factors such as temperature, humidity, pH value, organic reagents, and toxic chemicals.[18–21] To solve these problems, nonenzymatic glucose biosensors based on the direct detection of glucose have been developed for practical applications. Recent research has shown that nanomaterials can be applied as sensors for glucose detection because of their unique physical and chemical properties. For example, noble metals, metal alloys, and metal oxides have been successfully used in the construction of nonenzymatic glucose sensors,[22–28] suggesting that nanostructured materials are potential candidates for application as nonenzymatic glucose sensors.

As an important II–VI semiconductor material, ZnS has been extensively studied due to its luminescent, photochemical, and electrochemical properties.[29,30] NiS has also been widely studied and has widespread applications in lithium ion batteries, supercapacitors, waste water treatment, etc.[31–33] The individual physical and chemical properties of ZnS or NiS materials have been extensively studied; however, there have been few reports on ZnS–NiS composites as nonenzymatic glucose sensors.

Recently, much attention has been focused on improving the related physical and chemical performance of materials based on mixed transition metal sulfides, which can provide a synergistic effect of all individual constituents and efficient rapid pathways for ion and electron transport not only at the surface of materials, but also throughout the bulk of materials.[34–36] Although many simple metal sulfides have been prepared, the controllable preparation of mixed transition metal sulfides with desirable composition and morphology still

[a] Dr. C. Wei, C. Cheng, Dr. J. Zhao, Z. Wang, H. Wu, K. Gu, Prof. W. Du, Prof. H. Pang
College of Chemistry and Chemical Engineering
Anyang Normal University, Anyang, 455002 Henan (P. R. China)
E-mail: huanpangchem@hotmail.com
Homepage: http://huanpangchem.wix.com/advanced-material

[b] Prof. H. Pang
State Key Laboratory of Coordination Chemistry
Nanjing University, Nanjing, 210093 Jiangsu (P. R. China)

remains a great challenge. Thus, developing simple routes to prepare mixed transition metal sulfides is necessary.

In this work, we have successfully prepared mesoporous ZnS–NiS composites by ion-exchange reactions using ZnS as a precursor. The specific mesoporous ZnS–NiS composite has two advantages: 1) It provides a large enough inner space and a high active surface area due to a strong synergistic effect from ZnS and NiS; 2) As electrochemical active materials for nonenzymatic glucose sensors, the synthesized ZnS–NiS mesoporous composites show a low detection limit of 0.125 μM. Moreover, the sensor is also highly selective to the target analyte. The mesoporous ZnS–NiS composites hold potential in enzyme-free determination of glucose.

Results and Discussion

The synthesis of ZnS–NiS mesoporous materials was performed via a simple ion-exchange reaction between Ni^{2+} and ZnS nanospheres. Figure 1 presents the X-ray diffraction (XRD) patterns of the prepared samples. All the diffraction peaks can be perfectly indexed to the pure hexagonal phase of ZnS with lattice parameters $a = 0.3821$ nm and $c = 0.6257$ nm, which are in good agreement with the International Center for Diffraction Data's Joint Committee on Powder Diffraction Standards (JCPDS) card 36-1450. The XRD pattern shows that the diffraction peaks of (100) and (101) overlap with the diffraction peak of (002) because of widening, which is a result of the small crystallite size. No characteristic peaks corresponding to other impurities were observed in the pattern, which indicates that the products are pure ZnS (Figure 1 a). Figure 1 b shows the XRD pattern of the prepared ZnS–NiS composites. It is worth noting that there is no peak pertaining to NiS.

To gain further information on the elemental compositions of the ZnS–NiS composites, X-ray photoelectron spectroscopy (XPS) was used to further characterize the sample. Figure 2 b exhibits the Zn 2p XPS spectrum for the ZnS–NiS composite. The two strong peaks at 1020.8 and 1044.1 eV, assigned to the binding energies of Zn $2p_{3/2}$ and Zn $2p_{1/2}$, respectively, suggest the existence of Zn^{2+}.[34] The Ni 2p XPS spectrum is shown in Figure 2 c; two major peaks with binding energies at 855.3 and 872.8 eV are found, which correspond to Ni $2p_{3/2}$ and Ni $2p_{1/2}$, respectively. In addition, a weak peak corresponding to the satellite peak at around 861.2 eV was also observed, which was
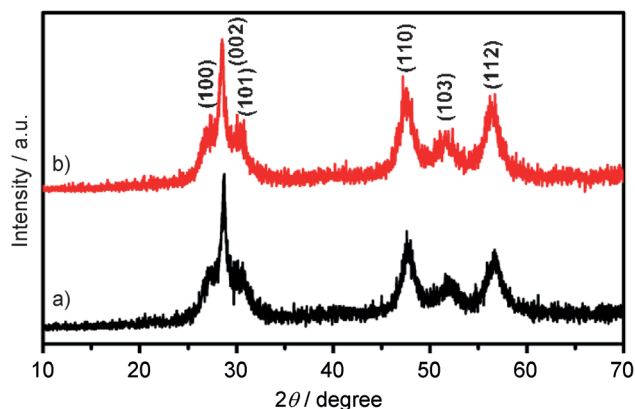

Figure 1. X-ray diffraction (XRD) patterns of a) ZnS and b) ZnS–NiS composite materials.

ascribed to the multi-electron excitation (shake-up signal).[37] High-resolution scans of the S element in Figure 2 d reveal a peak centered at around 160.6 eV, which can be accordingly assigned to the binding energy of S 2p.[35] The corresponding energy dispersive X-ray spectroscopy (EDS) maps of the ZnS–NiS composites were also recorded (Figure S1, Supporting Information) to further confirm the Zn, Ni, and S elements. In Figure S1 three color mapping images are shown: red: Zn–K, green: Ni–K, and blue: S–K. For the different element contents, the green Ni–K color is much lighter than the red Zn–K images, which reveals that the Ni content is much lower than the Zn content. Quantitative analysis of Ni element was also
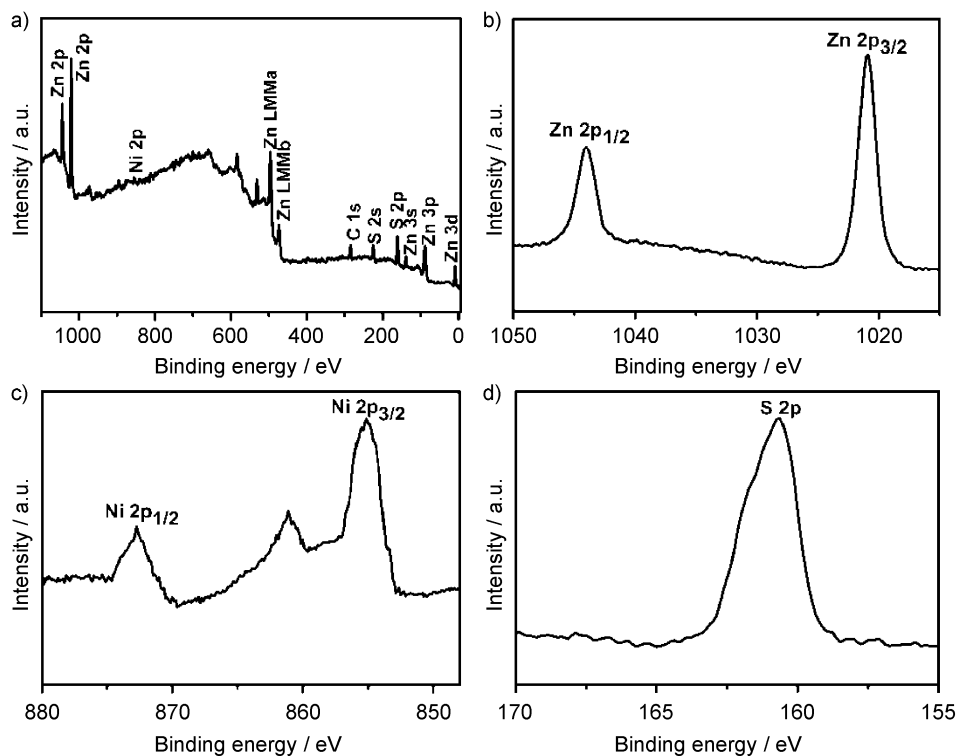

Figure 2. High resolution X-ray photoelectron spectroscopy (XPS) survey scan spectra of the ZnS–NiS composites: a) Full survey scan; b) Zn 2p; c) Ni 2p; d) S 2p.
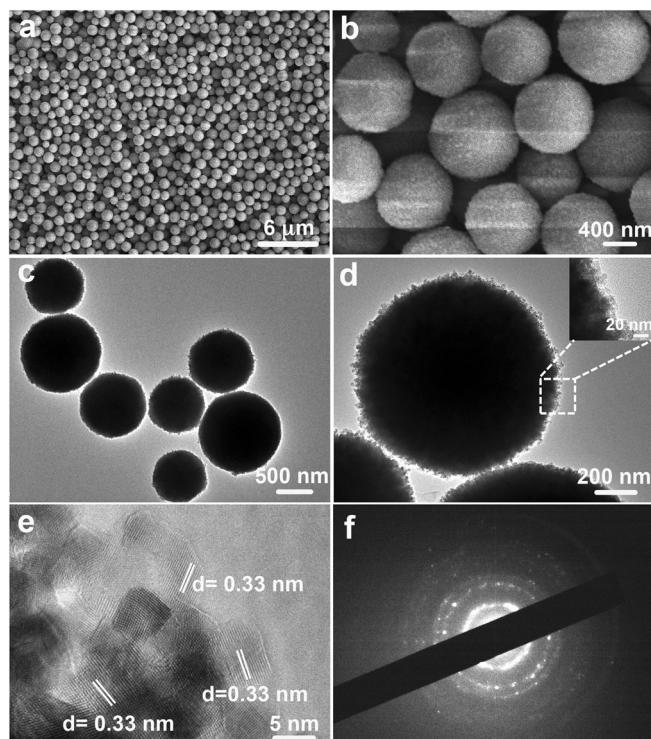
Figure 3. Scanning electron microscopy (SEM) images of ZnS (a,b); transmission electron microscopy (TEM) images of ZnS (c,d), inset: highly enlarged section of the image; e) high-resolution TEM image of the ZnS shell; f) selected area electron diffraction (SAED) patterns of ZnS.

Figure 4. Transmission electron microscopy (TEM) images of the ZnS–NiS composites (a–c); d) high-resolution TEM image of the area marked with a white circle in panel c.

Figure 5. a) N$_2$ adsorption–desorption isotherms of the prepared samples; b) corresponding pore volume distribution (dV dr^{-1}) against pore diameter curves of the prepared samples.

performed. It was found that the Ni element content is about 4.5 at%.

The morphology of ZnS and ZnS–NiS composites were investigated by electron microscopy. Typical scanning electron microscopy (SEM) and transmission electron microscopy (TEM) images are shown in Figure 3 a–d. The prepared ZnS particles are monodisperse solid spheres with average diameters of 500 nm, and the surfaces of these spheres are relatively rough (Figure 3 a,b), suggesting that the ZnS solid nanospheres contain a large number of packed nanoparticles, which is further confirmed by the corresponding highly enlarged TEM image (see inset in Figure 3 d). A high-resolution TEM image (Figure 3 e) displays several sets of lattice fringes with a spacing of 0.33 nm, corresponding to the (100) planes of hexagonal phase ZnS crystals. The selected area electron diffraction (SAED) patterns confirm that the obtained ZnS are polycrystalline. The detailed crystal structures of ZnS–NiS composites were also examined using TEM. The TEM image in Figure 4 a shows ZnS–NiS composite nanospheres with the diameter of about 500 nm. The surface of the ZnS–NiS composite nanospheres becomes rougher (Figure 4 b), suggesting the formation of NiS crystallites on the ZnS surface. The high-resolution TEM image of ZnS–NiS composites in Figure 4 d displays the lattice planes of ZnS (100) and NiS (110) with lattice spacings of 0.33 and 0.17 nm, respectively.

The specific surface areas and pore size of the prepared ZnS and ZnS–NiS composites were further studied by nitrogen adsorption–desorption measurements, as indicated in Figure 5.
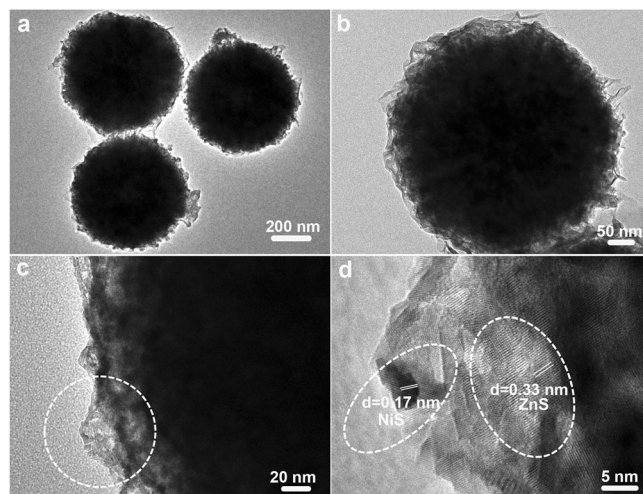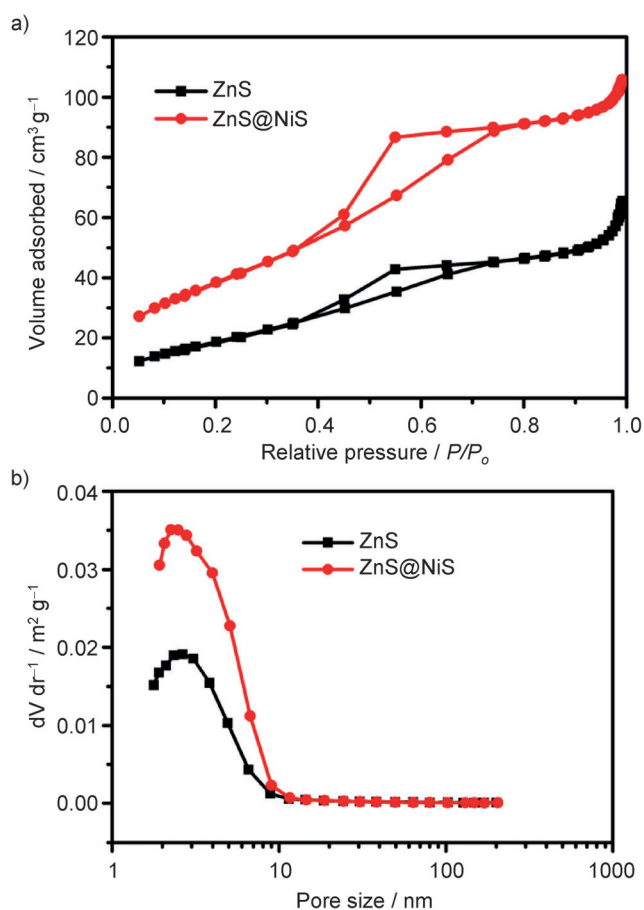
The hysteresis loop of the ZnS and ZnS–NiS composites typically belongs to type IV, indicating the characteristics of a mesoporous material. As shown in Figure 5 a, the specific surface

area of ZnS–NiS composites (137.9 m^{2}g^{-1}) is much larger than that of ZnS (68.9 m^{2}g^{-1}). The Barrett–Joyner–Halenda (BJH) pore size distribution curves (Figure 5b) show that the ZnS and ZnS–NiS composites present a monomodal pore distribution, and the average pore diameter is about 2.4 nm. As widely reported, a large effective surface area usually offers many nanochannels for contacting the electrolyte through surface–interface interactions of nanoporous micro-/nano-structures.[16,38,39] It is reasonable to conclude that mesoporous ZnS–NiS composites might have a potential application in glucose electrochemical sensors.

To evaluate the electrochemical property of the prepared mesoporous ZnS–NiS composites, we carried out the cyclic voltammetry (CV) to investigate glucose oxidation and reduction. Figure 6 presents the CV traces of mesoporous ZnS–NiS composites using a modified glassy carbon (GC) electrode and
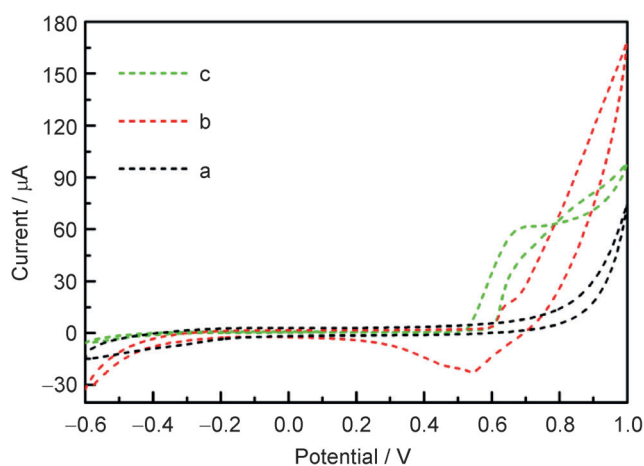

Figure 6. Cyclic voltammetry (CV) traces: a) bare GC electrode in glucose (5 mM) and NaOH (0.1 M); GC electrode modified with ZnS–NiS composites in NaOH (0.1 M) in the b) absence or c) presence of glucose (5 mM); Scan rate = 50 mV s^{-1}.

a bare GC electrode in the absence and presence of 5 mM glucose in 0.1 M NaOH. As shown for the bare GC electrode, there is only a small background current observed (Figure 6a), whereas a big increase in signal can be noted when the electrode was modified by the prepared mesoporous ZnS–NiS composites (Figure 6b). Upon the addition of 5 mM glucose, a more dramatic increase can be found after the GC electrode was modified (Figure 6c).

We also carried out CV to investigate glucose oxidation and reduction in physiological pH values (pH 7.2). After the addition of 5 mM glucose, a small increase of signal can be noted (Figure S2, Supporting Information). These results demonstrate that mesoporous ZnS–NiS composites have an excellent electroanalytical ability in 0.1 M NaOH solution compared with solutions at physiological pH and an enhanced response that can be attributed to many transport channels in the mesoporous ZnS–NiS composites materials owing to its high specific surface areas.

Current–time responses at a potential of 0.6 V after successive injections of different amounts of glucose into the 0.1 M

NaOH solution under stirring are presented in Figure 7a. It can be seen from the insets of Figure 7a that a GC electrode modified with mesoporous ZnS–NiS composites shows an obvious increase in current response after successive additions of glucose, and it takes less than 5 s to achieve the steady-state cur-
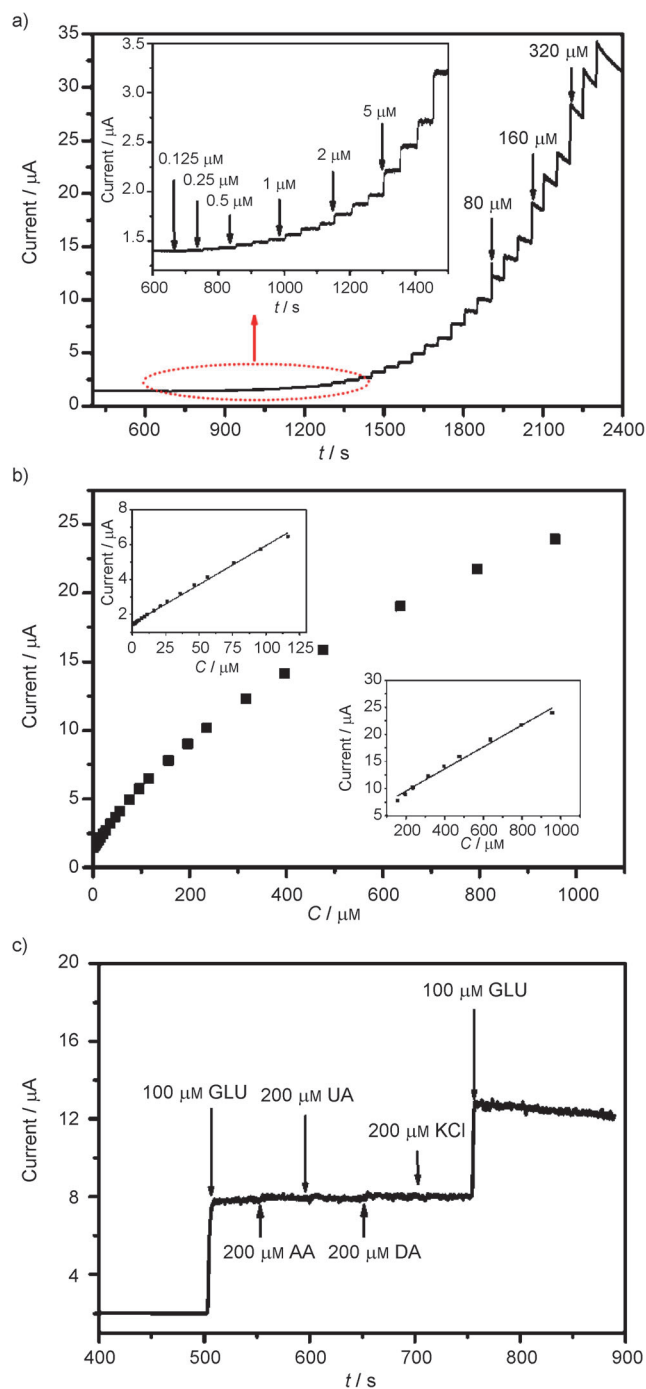

Figure 7. a) Current–time response diagram of a GC electrode modified with mesoporous ZnS–NiS composites upon successive addition of glucose in NaOH (0.1 M) (inset: magnified diagram at glucose concentrations of 0.125–5 μM); b) plot of electrocatalytic current of glucose versus its concentrations in the range of 0.125 μM–1.0 mM; c) amperometric response of modified electrodes with successive addition of glucose, ascorbic acid (AA), uric acid (UA), dopamine (DA), KCl, and glucose in NaOH (0.1 M).

rent upon addition of glucose to the stirring support electrolyte. The high catalytic activity of the GC electrode modified with mesoporous ZnS–NiS composites could be attributed to the synergistic effect of the composites, which include highly active catalytic sites for glucose oxidation owing to the high specific surface areas. The high electron-transfer rate can be associated with the many transport channels throughout the mesoporous ZnS–NiS composite materials. In Figure 7b, we find the glucose detection concentration range to be 0.125 μM–0.12 mM (R = 0.9968), and the calculated sensitivity is 48.5 μA mM^{-1}. In the glucose concentration range of 0.15 mM–1.0 mM (R = 0.9935), the calculated sensitivity is 26.4 μA mM^{-1}. The performance of the prepared mesoporous ZnS–NiS composites is comparable with some nonenzymatic glucose sensors, as shown in Table S1 (Supporting Information). The sensitivity and detection limit of glucose for the mesoporous ZnS–NiS composite electrocatalyst are better than those of many nonenzymatic sensors, such as PtNi nanoparticles/Graphene (20.42 μA mM^{-1} cm^{-2}, 0.01 mM),[40] palladium nanotube (33.19 μA mM^{-1}, 0.1 mM), and NiO/DNA-dispersed graphene hybrid (9 μA mM^{-1} cm^{-2}, 2.5 μM).[41,42] However, the sensitivity and detection limit of some nonenzymatic sensors are better than our results, such as for porous Ni networks (2900 μA mM^{-1} cm^{-2}, 0.07 μM)[43] and CuO–NiO microfibers (3165.53 μA mM^{-1} cm^{-2}, 1 nM).[44] The results confirm that mesoporous ZnS–NiS composites can be a promising functional material for the electroanalytical detection of glucose.

One of the major challenges in nonenzymatic glucose detection is to eliminate the electrochemical response generated by some easily oxidizable endogenous interfering compounds such as ascorbic acid (AA), uric acid (UA), dopamine (DA), and KCl. Owing to their higher electron transfer rates, these interfering species can produce the oxidation current comparable to that of glucose. It is expected that a mesoporous ZnS–NiS composite electrode with highly active surfaces can favor a kinetically controlled sluggish reaction (the oxidation of glucose) to a greater extent than diffusion-controlled reactions (the oxidation of interfering species). Therefore, interference tests were carried out by adding 100 μM glucose, followed with additions of 200 μM AA, 200 μM UA, 200 μM DA, and 200 μM KCl in 0.1 M NaOH. The results shown in Figure 7c demonstrate that almost negligible interference from AA, UA, DA, and KCl is present at the sensor. Mesoporous ZnS–NiS composites exhibit high selectivity, which is might attributed to the morphological characteristics of a mesoporous structure with high specific surface area and a rational composition of the two constituents. In addition, mesoporous ZnS–NiS composites on the surface of electrodes can be used to modify the mass transport regime, and under favorable circumstances, this alteration can facilitate the amperometric discrimination between species.[45–47] Thus, ZnS–NiS sensors exhibit high selectivity.

The reproducibility and stability of the sensor were evaluated. Seven electrodes modified with ZnS–NiS mesoporous materials were made, and their current responses to 10 μM glucose were investigated. The relative standard deviation (RSD) was 3.51% with a mean current response of 0.0739 μA. Figure 8 shows the stability of the ZnS–NiS/GC electrode's re-
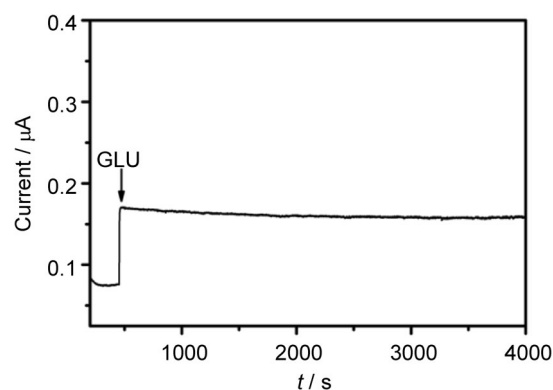

Figure 8. The stability of the response current for a GC electrode modified with ZnS–NiS composites after the addition of glucose (10 μM) measured over 4000 s.

sponse current over 4000 s after the addition of 10 μM glucose. After 4000 s, there is only a 6% loss in the specific response current of the electrode, which is stable enough for use as an electrochemical sensor of glucose.

Based on the discussion above, the prepared mesoporous ZnS–NiS composites exhibit good electrocatalytic activity towards glucose. Such a good electrochemical response capability in mesoporous ZnS–NiS composites might be explained as follows: First, the mesoporous ZnS–NiS composites can offer a larger accessible surface area for the nanopores, a short diffusion path for ions, and good conductivity. Secondly, mesoporous ZnS–NiS composites could have novel interfaces (between the ZnS and NiS nanoparticles), which can provide a synergistic effect from individual constituents and efficient, rapid pathways for ion and electron transport not only at the material's surface, but also throughout the bulk of the material. Different surface/interface characteristics and conductivity will lead to different chemical–physical adsorption–desorption abilities towards ions and their diffusion paths, resulting in a better electroanalytical detection of glucose.[48–50]

Conclusions

Mesoporous ZnS–NiS composites have been prepared by ion-exchange reactions using ZnS as a precursor. As a result of novel interface characteristics, conductivity, and synergistic effects from ZnS and NiS constituents, the mesoporous ZnS–NiS composites provide an efficient and rapid pathway for ion and electron transport not only at the material's surface, but also throughout the bulk of the material. We have successfully explored the application of the mesoporous ZnS–NiS composites in the enzyme-free detection of glucose. The results of the electrochemical detection show the mesoporous ZnS–NiS composites exhibit high selectivity and a low detection limit for the oxidation of glucose. This present study is important as it provides us with an effective approach in preparing novel mesoporous ZnS–NiS composites that are useful as electroactive materials for the nonenzymatic sensing of glucose. This synthesis method can be extended to the preparation of other materials for many applications.

Experimental Section

Materials preparation: ZnS nanospheres were prepared as follows: $Zn(Ac)_2 \cdot 6H_2O$ (0.5 mmol) was dissolved in glycerol (8.0 mL) and H_2O (9.0 mL) with magnetic stirring, then NH_3 solution (3.0 mL, 25%, analytically pure) and L-cysteine (3.0 mmol) were added, respectively. After 10 min of stirring at RT, the mixture was transferred into a 50 mL Teflon-lined autoclave reactor and heated in an oven at 140 °C for 6 h. The precipitate was centrifuged (4000 rpm for 10 min) and washed with deionized H_2O (10 mL) and absolute ethanol (10 mL), and dried in a vacuum oven at 50 °C for 12 h.

To prepare ZnS–NiS mesoporous composites, ZnS (1.0 mmol) nanospheres were dispersed in deionized H_2O (20 mL). Then, $Ni(Ac)_2 \cdot 4H_2O$ (248.8 mg, 1.0 mmol) was added to the solution while stirring. The resulting mixture was then transferred into a 100 mL round-bottom flask and heated at 80 °C for 24 h using a water bath. The precipitate was collected by centrifugation (4000 rpm for 10 min) and washed with deionized H_2O (10 mL) and absolute ethanol (10 mL), then dried at 50 °C for 12 h.

Preparation of the glucose sensor: The glassy carbon (GC) electrode (3 mm diameter) was carefully polished using a polishing cloth with alumina slurry (1.0, 0.3, and 0.05 μm in sequence), then rinsed thoroughly with deionized H_2O, and allowed to dry at RT. To prepare the GC electrode modified with the ZnS–NiS mesoporous material, an aqueous dispersion of the ZnS–NiS composite (1 mg mL^{-1}) was prepared, and the suspension (5 μL) was cast onto the surface of the pretreated GC electrode. The solvent was allowed to evaporate at RT, leaving the ZnS–NiS mesoporous material immobilized on the GC electrode surface.

Apparatus and measurements: Cyclic voltammetry (CV) measurements were performed on a CHI 660D electrochemical station (Chen Hua, Shanghai, China), a three-compartment electrochemical cell containing a saturated calomel reference electrode, a platinum wire auxiliary electrode, and a modified GC electrode as the working electrode. Glucose measurement was carried out in 0.1 M NaOH at RT. For the CV measurements, the potential scan was taken from −0.60 to 1.00 V at a scan rate of 50 mV s^{-1}. For the amperometric detection, all measurements were performed by applying an appropriate potential to the working electrode and allowing the transient background current to decay to a steady-state value prior to the addition of glucose. The current response was recorded at the addition of glucose.

Characterization: The morphology of the obtained sample was observed by a Hitachi S-4800 field emission scanning electron microscope (FE-SEM) at an acceleration voltage of 10.0 kV. The phase analyses of the samples were characterized by X-ray diffraction (XRD) on a Shimadzu XRD-6000 powder X-ray diffractometer with Cu-Kα radiation ($\lambda = 1.5418$ Å). Standard and high-resolution (HR) transmission electron microscopy (TEM) images were obtained on a JEOL JEM-2100 microscope at an acceleration voltage of 200 kV. The surface area, pore size, and pore size distribution of the materials were determined by Brunauer–Emmett–Teller (BET) nitrogen adsorption–desorption and Barett–Joyner–Halenda (BJH) methods on a Micromimetrics ASAP2020 physisorption analyzer.

Acknowledgements

[1] M. H. Cao, T. F. Liu, S. Gao, G. B. Song, X. L. Wu, C. W. Hu, Z. L. Wang, *Angew. Chem. Int. Ed.* **2005**, *44*, 4197–4201; *Angew. Chem.* **2005**, *117*, 4269–4273.

[2] C. Z. Wei, C. Cheng, J. H. Zhao, S. S. Zheng, M. M. Hao, H. Pang, *Dalton Trans.* **2014**, *43*, 5687–5693.

[3] C. Wei, H. Pang, B. Zhang, Q. Lu, S. Liang, F. Gao, *Sci. Rep.* **2013**, *3*, 2193.

[4] H. Jiang, T. Zhao, C. Z. Li, J. Ma, *J. Mater. Chem.* **2011**, *21*, 3818–3823.

[5] J. P. Liu, X. T. Huang, Y. Y. Li, K. M. Sulieman, X. He, F. L. Sun, *Cryst. Growth Des.* **2006**, *6*, 1690–1696.

[6] M. Han, Q. Liu, J. H. Liu, Y. Song, Z. Xu, J. M. Zhu, *Adv. Mater.* **2007**, *19*, 1096–1100.

[7] W. Li, L. Kuai, Q. Qin, B. Y. Geng, *J. Mater. Chem. A* **2013**, *1*, 7111–7117.

[8] J. F. Liu, L. L. Wang, X. M. Sun, X. Q. Zhu, *Angew. Chem. Int. Ed.* **2010**, *49*, 3492–3495; *Angew. Chem.* **2010**, *122*, 3570–3573.

[9] G. X. Zhu, Z. Xu, *J. Am. Chem. Soc.* **2011**, *133*, 148–157.

[10] J. W. Qin, J. F. Lu, M. H. Cao, C. W. Hu, *Nanoscale* **2010**, *2*, 2739–2743.

[11] X. J. Zhang, A. X. Gu, G. F. Wang, Y. Huang, H. Q. Ji, B. Fang, *Analyst* **2011**, *136*, 5175–5180.

[12] Y. Hou, J. C. Ndamanisha, L. P. Guo, X. J. Peng, J. Bai, *Electrochim. Acta* **2009**, *54*, 6166–6171.

[13] Y. Fu, J. M. Song, Y. Q. Zhu, C. B. Cao, *J. Power Sources.* **2014**, *262*, 344–348.

[14] X. Xia, Q. Hao, W. Lei, W. Wang, D. Sun, X. Wang, *J. Mater. Chem.* **2012**, *22*, 16844–16850.

[15] C. Z. Yuan, X. G. Zhang, L. H. Su, B. Gao, L. F. Shen, *J. Mater. Chem.* **2009**, *19*, 5772–5777.

[16] C. Z. Wei, Y. Y. Liu, X. R. Li, J. H. Zhao, Z. Run, H. Pang, *ChemElectroChem* **2014**, *1*, 799–807.

[17] A. Safavi, S. N. Maleki, E. Farjami, *Biosens. Bioelectron.* **2009**, *24*, 1655–1660.

[18] S. Liu, B. Yu, T. Zhang, *Electrochim. Acta* **2013**, *102*, 104–107.

[19] D. Lee, J. Lee, J. Kim, J. Kim, H. B. Na, B. Kim, C. H. Shin, J. H. Kwak, A. Dohnalkova, J. W. Grate, T. Hyeon, H. S. Kim, *Adv. Mater.* **2005**, *17*, 2828–2833.

[20] E. Reitz, W. Jia, M. Gentile, Y. Wang, Y. Lei, *Electroanalysis* **2008**, *20*, 2482–2486.

[21] J. Wang, *Chem. Rev.* **2008**, *108*, 814–825.

[22] Y. Y. Song, D. Zhang, W. Cao, X. H. Xia, *Chem. Eur. J.* **2005**, *11*, 2177–2182.

[23] J. P. Wang, D. F. Thomas, A. C. Chen, *Anal. Chem.* **2008**, *80*, 997–1004.

[24] Y. Mu, D. L. Jia, Y. Y. He, Y. Q. Miao, H. L. Wu, *Biosens. Bioelectron.* **2011**, *26*, 2948–2952.

[25] Y. Y. Liu, Y. J. Zhang, T. Wang, P. P. Qin, Q. F. Guo, H. Pang, *RSC Adv.* **2014**, *4*, 33514–33519.

[26] H. Pang, Q. Y. Lu, J. J. Wang, Y. C. Li, F. Gao, *Chem. Commun.* **2010**, *46*, 2010–2012.

[27] K. E. Toghill, R. G. Compton, *Int. J. Electrochem. Sci.* **2010**, *5*, 1246–1301.

[28] K. Tian, M. Prestgard, A. Tiwari, *Mater. Sci. Eng. C* **2014**, *41*, 100–118.

[29] X. X. Yu, J. G. Yu, B. Cheng, B. B. Huang, *Chem. Eur. J.* **2009**, *15*, 6731–6739.

[30] M. Jayalakshmi, M. M. Rao, *J. Power Sources.* **2006**, *157*, 624–629.

[31] J. Q. Yang, X. C. Duan, Q. Qin, W. J. Zheng, *J. Mater. Chem. A* **2013**, *1*, 7880–7884.

[32] Y. Wang, Q. S. Zhu, L. Tao, X. W. Su, *J. Mater. Chem.* **2011**, *21*, 9248–9254.

[33] C. Z. Wei, Q. Y. Lu, J. Sun, F. Gao, *Nanoscale* **2013**, *5*, 12224–12230.

[34] J. G. Yu, J. Zhang, S. W. Liu, *J. Phys. Chem. C* **2010**, *114*, 13642–13649.

[35] Y. H. Shi, Y. J. Chen, G. H. Tian, H. G. Fu, K. Pan, J. Zhou, H. J. Yan, *Dalton Trans.* **2014**, *43*, 12396–12404.

[36] Z. Fang, Y. F. Liu, Y. T. Fan, Y. H. Ni, X. W. Wei, K. B. Tang, J. M. Shen, Y. Chen, *J. Phys. Chem. C* **2011**, *115*, 13968–13976.

[37] H. Pang, C. Z. Wei, Y. H. Ma, S. S. Zhao, G. C. Li, J. S. Zhang, J. Chen, S. J. Li, *ChemPlusChem* **2013**, *78*, 546–553.

[38] X. W. Li, S. L. Xiong, J. F. Li, J. Bai, Y. T. Qian, *J. Mater. Chem.* **2012**, *22*, 14276–14283.

[39] L. J. Han, R. J. Liu, C. S. Li, H. H. Li, C. X. Li, G. J. Zhang, J. N. Yao, *J. Mater. Chem.* **2012**, *22*, 17079–17085.

[40] H. C. Gao, F. Xiao, C. B. Ching, H. W. Duan, *ACS Appl. Mater. Interfaces* **2011**, *3*, 3049–3057.

[41] J. Chen, W. D. Zhang, J. S. Ye, *Electrochem. Commun.* **2008**, *10*, 1268–1271.

[42] V. Lv, F. M. Jin, Q. G. Guo, Q. H. Yang, F. Y. Kang, *Electrochim. Acta* **2012**, *73*, 129–135.

[43] X. Zhu, Q. Jiao, C. Zhang, X. Zuo, X. Xiao, Y. Liang, J. Nan, *Microchim. Acta* **2013**, *180*, 477–483.

[44] F. Cao, S. Guo, H. Y. Ma, G. C. Yang, S. X. Yang, J. Geng, *Talanta* **2011**, *86*, 214–220.

[45] M. C. Henstridge, E. F. Dickinson, M. Aslanoglu, C. B. McAuley, R. G. Compton, *Sens. Actuators B* **2010**, *145*, 417–427.

[46] I. Streeter, G. G. Wildgoose, S. L. Dong, R. G. Compton, *Sens. Actuators B* **2008**, *133*, 462–466.

[47] M. J. Sims, N. V. Rees, E. F. Dickinson, R. G. Compton, *Sens. Actuators B* **2010**, *144*, 153–158.

[48] C. Z. Wei, H. Pang, C. Cheng, J. H. Zhao, P. W. Li, Y. K. Zhang, *CrystEngComm* **2014**, *16*, 4169–4175.

[49] L. Xu, R. F. Zheng, S. H. Liu, J. Song, J. S. Chen, B. Dong, H. W. Song, *Inorg. Chem.* **2012**, *51*, 7733–7740.

[50] L. J. Lauhon, M. S. Gudiksen, D. Wang, C. M. Lieber, *Nature* **2002**, *420*, 57–61.